Additional Information

1 **PASSIVITY BREAKDOWN OF TITANIUM IN LiBr SOLUTIONS**

2

3 **Fernández-Domene, R.M., Blasco-Tamarit, E., García-García, D.M., García-**

4 **Antón, J. ***

5 *Ingeniería Electroquímica y Corrosión (IEC). Departamento de Ingeniería Química y*

6 *Nuclear. ETSI Industriales. Universitat Politècnica de València. Camino de Vera s/n,*

7 *46022 Valencia, Spain.*

8 *Corresponding author. Tel. 34-96-387 76 32, Fax. 34-96-387 76 39,*

9 *e-mail: jgarciaa@iqn.upv.es (J. García-Antón); raferdo1@etsii.upv.es (R.M.*

10 *Fernández-Domene).*

11

12

13 The passive behavior of titanium and its susceptibility to undergo localized attacks in

14 different LiBr solutions at 25º C have been investigated using different electrochemical

15 techniques: potentiodynamic polarization curves, potentiostatic passivation tests, EIS

16 measurements and Mott-Schottky analysis. In low and moderately concentrated LiBr

17 solutions, the breakdown potential E_b decreased with increasing bromide

18 concentrations, while in highly concentrated LiBr solutions, E_b increased with

19 increasing LiBr concentration. In the most concentrated LiBr solution (11.42M) Ti did

20 not undergo passivity breakdown even at 9 $V_{Ag/AgCl}$. These results have been related to a

21 decrease in the activity of water in highly concentrated LiBr solutions.

22

23

1

1. INTRODUCTION

Titanium is a very reactive metal that shows remarkable corrosion resistance in many environments due to the formation of a very stable, continuous, highly adherent, and protective passive oxide film on the metal surface. A freshly abraded titanium surface immediately passivates when exposed to an oxygen source (air and/or moisture). The nature, composition, and thickness of the passive film that forms on titanium depend on the environmental conditions. In most aqueous environments, the oxide is typically TiO_2, but may consist of mixtures of other titanium oxides, including TiO_2, Ti_2O_3, and TiO [1-8]. The oxygen content of the titanium oxide gradually decreases from TiO_2 at the surface, to Ti_2O_3 and TiO as it approaches the metal/oxide interface [1]. Depending on the environment, this oxide may be covered with an amorphous or hydrated surface oxide, giving a two-layer oxide structure [1, 4, 5, 9]. The TiO_2 passive film is an n-type semiconductor and its semiconductive properties determine the current/potential behavior of the titanium/passive film/electrolyte system [1, 6, 10-13]. The metal/passive film interface has been assumed to be an ohmic contact with minimal resistance. On the other hand, a space charge region has been hypothesized to develop at the passive film/electrolyte interface [6]. Oxygen vacancies have been reported to be the main defects within the passive film on titanium [13-15]. Ti^{3+} interstitials have also been cited as electron donor species [10, 12].

Titanium exhibits excellent resistance to most salt solutions over a wide range of pH and temperatures [16]. Although titanium is resistant to these media, it is not immune and can be susceptible to pitting and crevice attack, depending on the environmental conditions [15-18]. Breakdown potentials (E_b) of titanium in sulfate and phosphate

media are typically in excess of 80 V_{SCE} [1, 19]. Values of 5 to 12 V_{SCE} can be expected in room-temperature chloride solutions [1, 15, 18, 19]. However, it has been observed in numerous works that bromide anions are far more effective than chlorides or iodides in facilitating breakdown of the passive film formed on Ti [15, 17-22]. In fact, many authors have observed passivity breakdown of titanium in bromide containing solutions taking place at relatively low potentials compared to those in chloride or iodide containing solutions (E_b < 2-5 V_{SCE}) [15, 17-24]. Sazou et al. [15] interpreted this high susceptibility of TiO_2 to local breakdown in the presence of bromides by considering electrochemical reactions taking place at the passive film/electrolyte interface, such as the formation of surface titanium peroxo-species, leading to changes in the surface and bulk properties (ionic and electronic) of the titanium oxide. The breakdown potential of titanium in relatively low concentrated bromide solutions (up to 1M) has been found to decrease with increasing bromide concentrations [15, 18, 20], with values in the range of 2-5 $V_{Ag/AgCl}$. Nevertheless, it has been observed in recent works [2, 25] that in very concentrated LiBr solutions (700, 850 and 992 g/l LiBr, 8.06M, 9.78M and 11.42, respectively), titanium did not undergo localized attacks at potentials as high as $3V_{Ag/AgCl}$. These results contradict the tendencies found in the literature for E_b with bromide concentration, since in heavy brine LiBr solutions the values of E_b should be lower than 2-3 $V_{Ag/AgCl}$.

The aim of the present work is to study the influence of bromide concentration on the passivity breakdown of titanium at 25º C and to clarify the anomalous behavior of passive films formed on titanium in highly concentrated LiBr solutions against localized attacks. These heavy brine LiBr solutions are widely used in absorption cooling systems [26-30]. The steady-state properties of the passive film formed on Ti electrodes in

76   different LiBr solutions have been studied in this work, as well as the role of electronic

77   properties and the activity of water on the stability of Ti passive film.

78

79   **2. MATERIALS AND METHODS**

80

81   *Materials, solution and electrochemical cell*

82

83   The material tested was commercially pure Grade 2 titanium (0.03 wt.% N, 0.1 wt.% C,

84   0.25 wt.% O, 0.3 wt.% Fe, 0.0125 wt.% H, Bal. Ti). Titanium electrodes were

85   cylindrically shaped and covered with a polytetrafluoroethylene (PTFE) coating, to

86   expose an area of 0.5 cm^2 to the test solution. All specimens were wet abraded from 200

87   to 4000 SiC grit, and finally rinsed with distilled water and air-dried. Titanium

88   electrodes were tested in different LiBr solutions, from 0.05M to 11.42M, at a constant

89   temperature of 25º C (**Table 1**). Values of molalities (m_{LiBr}), mean ionic activity

90   coefficients ($\gamma_\pm$), activities of LiBr solutions (a_{LiBr}), osmotic coefficients (ϕ) and

91   activities of water (a_W) are also shown in **Table 1**. Activities for LiBr solutions, a_{LiBr},

92   have been calculated from the following equation:

93

94    $$a_{LiBr} = \frac{m_{LiBr}}{m^0} \gamma_\pm \qquad \qquad \textbf{(1)}$$

95

96   where the LiBr molality, m_{LiBr}, is defined as mol LiBr/kg H_2O and m^0 is the standard

97   LiBr molality (m^0 = 1 mol LiBr/kg H_2O). Activity coefficients and osmotic coefficients

98   have been obtained from the literature [31]. Activities of water have been calculated

99   from osmotic coefficients according to the following expression [32, 33]:

100

101 $$\ln(a_W) = -\phi M_W \nu m \qquad \qquad \textbf{(2)}$$

102

103 where M_W is the molar mass of water and ν is the stoichiometric parameter, i.e., the

104 number of ion moles produced by complete dissociation of one mole of salt (for a 1:1

105 salt such as LiBr, ν equals 2); notice that molality m is expressed in kilomole of solute

106 per kilogram of solvent (or mole of solute per gram of solvent) so the units in eq. (2) are

107 consistent.

108

109 To study the effect of solvent nature and the influence of the bromide salt on the

110 passivity breakdown of Ti, additional experiments were carried out in different

111 electrolytes: 0.5M LiBr solutions with different water-methanol proportions (70 mol%,

112 50 mol% and 0 mol% water), and a 3M KBr solution.

113

114 The electrochemical tests were performed in a sheathed vertical electrochemical cell. A

115 silver-silver chloride (Ag/AgCl 3M KCl) was used as reference electrode and a

116 platinum wire as auxiliary electrode. Electrochemical measurements were performed

117 using an Autolab PGSTAT302N potentiostat. In all cases the tests were repeated at least

118 three times in order to verify reproducibility.

119

120 *Potentiodynamic polarization curves*

121

122 Polarization tests began at a cathodic potential value of -0.9 $V_{Ag/AgCl}$ and the potential

123 was subsequently scanned anodically at a scan rate of 0.5 mV s^{-1}. The passive current

124 density, i_p, and the breakdown potential, E_b (defined as the potential at which the current

125 density increases abruptly after the peak corresponding to the Br$^-$/Br$_2$ oxidation), were

5

126   obtained from potentiodynamic polarization tests. After potentiodynamic polarization,

127   the morphological inspection of the Ti electrodes surface was done using a Leica DM

128   LA optical microscope.

129

130   *Potentiostatic passivation tests*

131

132   Before the potentiostatic passivation experiments, the surface of the Ti electrodes was

133   pretreated cathodically at -0.9 $V_{Ag/AgCl}$ for 30 min to create reproducible initial

134   conditions. Afterwards, the working electrode was polarized at a potential within the

135   passive region of titanium (0.4 $V_{Ag/AgCl}$) for 1 hour in several LiBr solutions (0.1M,

136   0.5M, 3M and 11.42M) at 25º C, to form a stable passive film. During passivation

137   experiments, transients in the current density were recorded against time.

138

139   *EIS and capacitance measurements*

140

141   EIS and capacitance measurements were performed under potentiostatic conditions after

142   the passivation tests, once a stable passive film was formed on the surface of the Ti

143   samples. EIS measurements were conducted using a sinusoidal signal of 10 mV in

144   amplitude in the frequency range of 100 kHz-10 mHz. Capacitance measurements were

145   performed at a frequency of 10 kHz applying a sinusoidal potential perturbation of 10

146   mV and scanning the potential from the formation value in the negative direction at a

147   rate of 25 mV s^{-1}.

148

149   **3. RESULTS AND DISCUSSION**

150

151 **Potentiodynamic polarization curves**

152

153 The potentiodynamic polarization curves obtained for Ti in different LiBr solutions at

154 25º C are shown in **Figure 1**. A wide passive range can be observed in all LiBr

155 solutions where passive current density values (i_p) remain very low (of the order of 1-3

156 μA cm^{-2}), indicating the excellent passive behavior of Ti (**Table 2**). The values of i_p

157 have been estimated at a potential of 0.4 V, within the stable passive region. At first, i_p

158 slightly increases with increasing LiBr concentrations, but at concentrations higher than

159 0.7 M it starts decreasing until reaching its lowest value (1 μA cm^{-2}) in the 11.42 LiBr

160 solution.

161

162 Upon increasing the anodic polarization of Ti, the occurrence of a broad anodic wave

163 can be observed at potentials between 1-1.5 V, corresponding to the oxidation of

164 bromides present in the solution (E^0 (Br$_2$/Br$^-$) = 0.89 V$_{Ag/AgCl}$). This anodic wave is more

165 evident at high LiBr concentrations. In fact, in the potential range between 1-1.5 V a

166 change of the solution color around the titanium electrode surface (from colorless to

167 yellow-orange) was noticeable at high LiBr concentrations. This change in color is

168 related to the localized oxidation of bromide ions to bromine (Br$_2$) at electroactive sites

169 at potentials around 1.5 V$_{Ag/AgCl}$ [15, 17-20, 22] and to the subsequent formation of

170 HBrO, according to the following equations [34]:

171

172 $$2Br^- \Leftrightarrow Br_2 + 2e^- \tag{3a}$$

173

174 $$Br_2 + H_2O \rightarrow HBrO + Br^- + H^+ \tag{3b}$$
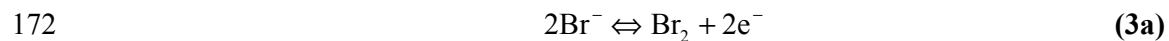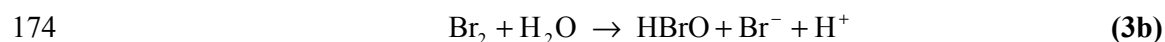
175

176 Apart from the oxidation of Br^-, several processes may take place simultaneously during

177 anodic polarization of titanium at high potentials, such as oxygen evolution reaction

178 (OER) [2, 19, 21, 23, 25, 35], oxidation of TiO and Ti_2O_3 to TiO_2 [2, 3, 5, 25, 35] or

179 additional oxidation of TiO_2 to form soluble complex species, such as TiO^{2+} [36],

180 or/and peroxo-species, such as TiO_3 or TiOOH [7, 8, 10, 15].

181

182 The abrupt increase of current density at potentials above the Br^- oxidation peak

183 indicates the onset of passivity breakdown of Ti. Once exposed to the Br^- solution, the

184 Ti metal rapidly oxidizes to a soluble oxi-halide Ti^{4+} species [18, 23]. In the low and

185 moderately concentrated LiBr solutions (**Figure 1a**) a decrease of E_b with increasing

186 bromide concentration can be observed, as reported in the literature [15, 18, 20] (**Table**

187 **2**). In the more concentrated LiBr solutions (**Figure 1b**), on the other hand, E_b does not

188 follow the previous tendency, since its value increases with increasing LiBr

189 concentration (**Table 2**). In fact, in the 11.42M LiBr solution Ti did not undergo

190 localized attacks under the experimental conditions (up to 9 $V_{Ag/AgCl}$), indicating that E_b

191 is apparently higher than 9 $V_{Ag/AgCl}$, which is a behavior more typical of chloride- or

192 iodide- than bromide-containing solutions [18]. A similar behavior was observed by

193 Davydov for niobium in LiBr solutions [37]. By way of illustration, **Figure 2** shows the

194 images of the Ti electrode surface before and after the polarization tests in 0.5M

195 (**Figure 2a**) and 11.42M (**Figure 2b**) LiBr solution. Visual inspection of the Ti

196 electrode polarized in the 0.5M LiBr solution (**Figure 2a**) reveals the presence of

197 several large corrosion pits. On the other hand, no damage is observed on the Ti

198 electrode polarized in the 11.42M LiBr solution up to 9 V (**Figure 2b**), in accordance

199 with the description of the polarization curves made above.

200

201   **Figure 3** shows the plot of E_b vs. the logarithm of bromide activity (log a_{Br^-}) for all the

202   LiBr solutions under study. It can be observed that E_b decreases linearly with log a_{Br^-}

203   for the low and moderately concentrated LiBr solutions, while it increases linearly with

204   log a_{Br^-} for the highly concentrated LiBr solutions (except in the 11.42M LiBr solution,

205   where passivity breakdown was not observed at all under the experimental conditions,

206   as commented above). The linear relationship with negative slope between E_b and log

207   a_{Br^-} (in low and moderately concentrated LiBr solutions) has been predicted analytically

208   by the Point Defect Model (PDM) [38, 39], according to the following equation:

209

210    $$E_b = \left(\frac{4.606RT}{\chi\alpha F}\right)\log\left(\frac{b}{D}\right) - \frac{2.303RT}{\alpha F}\log\left(a_{Br^-}\right) \tag{4}$$

211

212   where χ is the charge of the metal ions (Ti^{4+}), α is the polarizability of the passive

213   film/solution interface, F is Faraday's constant (96485.34 C mol^{-1}), b is a constant, D is

214   the diffusivity of cation vacancies in the passive film, R is the gas constant and T is

215   absolute temperature. From the straight line with negative slope shown in **Figure 3**, the

216   value of α can be determined, yielding a value of 0.045. This low value is comparable to

217   those reported in the literature for Ti [13, 15]. A low value of α suggests that the

218   Helmholtz layer is very weakly polarized since the potential drop at the passive

219   film/solution interface is negligible. Thus, almost all the potential drop in the interfacial

220   regions takes place in the metal/passive film interface, where the reaction of passive

221   film formation and growth occurs according to the PDM [40-42].

222

223   **Potentiostatic passivation tests**

224

225 The current density transients obtained after applying a potential step from a value of

226 -0.9 V (cathodic pre-treatment) to a value of 0.4 V within the passive region are shown

227 in **Figure 4** for different LiBr solutions (0.1M, 0.5M, 3M and 11.42M). It can be

228 observed that current densities follow the same tendency as i_p, that is, the order from

229 highest to lowest values during the whole potentiostatic test is: 0.5M, 3M, 0.1M and

230 11.43 LiBr solutions. In all cases, current density values decrease exponentially with

231 passivation, and eventually reach a steady-state value (i_{SS}). These values are the

232 following: 0.12 ± 0.05 μA cm^{-2} (0.1M), 0.22 ± 0.07 μA cm^{-2} (0.5M), 0.17 ± 0.05 μA cm^{-2}

233 (3M) and 0.059 ± 0.03 μA cm^{-2} (11.42M). Virtanen and Curty [20] observed a clear

234 increase in passive current density with increasing bromide concentrations for Ti in

235 NaBr. However, in the present study, i_{SS} increases with Br⁻ concentration at relatively

236 low concentrations, but it decreases with concentration at high LiBr concentrations.

237

238 According to the PDM [42-44], the steady-state current density can be written as:

239

240
$$i_{SS} = \delta F \left[k_{\text{int}} + k_{cat} + k_{dis} \left(\frac{C_{H^+}}{C_{H^+}^0} \right)^n \right]$$
(5)

241

242 where δ is the charge of the cation ejected from the passive film (3 in the case of Cr^{3+}),

243 C_{H^+} is the proton concentration in the solution, $C_{H^+}^0$ is a standard state H^+ concentration

244 and n is the kinetic order of the reaction of passive film dissolution with respect to

245 $\left(C_{H^+}/C_{H^+}^0 \right)$. The parameters k_{int}, k_{cat} and k_{dis} are the rate coefficients for the reactions of

246 formation of cation interstitials, cation vacancies and of passive film dissolution,

247 respectively. Eq. (5) suggests that the steady-state current density i_{SS} is associated with

248 the fluxes of point defects and also with the kinetic parameters for the interfacial

10

249   reactions. Hence, i_{SS} consists of three components: the first ($\delta F k_{int}$) resulting from the

250   generation and transport of cation interstitials, the second ($\delta F k_{cat}$) resulting from the

251   generation and transport of cation vacancies and the third $\delta F k_{dis}\left(C_{H^+}/C_{H^+}^0\right)^n$ resulting

252   from the movement of oxygen vacancies. The latter term is expressed in terms of the

253   dissolution rate of the passive film [42-45].

254

255   The passive film on titanium is well known to behave as an *n*-type semiconductor [1, 6,

256   10-13] (see Mott-Schottky analysis below), whose donor species are oxygen vacancies

257   and/or Ti^{3+} interstitials [10, 12-15], so the term related to the generation and transport of

258   cation vacancies, k_{cat}, can be neglected [43]. Therefore, the differences between current

259   densities with LiBr concentration are either due to the process of generation and

260   transport of cation interstitials or the dissolution of the passive film closely related to

261   the generation and movement of oxygen vacancies in the steady-state [41].

262

263
264   **Mott-Schottky analysis**
265
266
267
268   In order to check if the differences observed in i_{SS} at different LiBr concentrations is

269   due to the generation of donor species at the metal/passive film interface (oxygen

270   vacancies and/or cation interstitials), the electrochemical capacitance of the passive

271   system was measured as a function of the applied potential. Mott-Schottky (M-S)

272   analysis was performed to obtain the donor density, N_D, of the passive films formed on

273   Ti in different LiBr solutions. The total capacitance has been calculated from the

274   imaginary component of the impedance (Z'') using the relationship $C = -1/\omega Z''$, where ω

275   is the angular frequency.

276

277   As an illustration, **Figure 5** shows the capacitance-potential curves obtained for Ti in

278   the 0.5M LiBr solution at 0.4 V and at different frequencies. It is clearly observed that

279   capacitance values depend strongly on frequency. Capacitance-potential curves shift to

280   lower values with increasing frequencies. Such behavior has been frequently observed

281   for semiconducting passive films formed on metals and alloys [12, 46-54]. Several

282   physical explanations have been suggested in the literature as possible sources of this

283   dependence [46-54], such as the presence of deep donor states, contribution of surface

284   states, surface roughness, ionic charges movement, frequency dependant dielectric

285   constant, etc. It can be seen from **Figure 5** that capacitance becomes almost

286   independent of frequency at approximately 10 kHz. Therefore, a value of 10 kHz has

287   been used in this work to eliminate capacitance dependence on frequency.

288

289   **Figure 6** shows the Mott-Schottky plots at a frequency of 10 kHz of the passive film

290   formed on Ti in 0.1M, 0.5M, 3M and 11.42M LiBr solutions at 0.4 V. The positive

291   slopes of the M-S plots are characteristic of *n*-type semiconductors, with the dominant

292   defects in the passive film being oxygen vacancies and/or Ti^{3+} interstitials, as it has

293   been mentioned above.

294

295   The donor density, N_D, can be determined from the slopes in the M-S plots, according to

296   the following equation [10, 12]:

297

298   $$N_D = \frac{2}{\varepsilon \varepsilon_0 e \sigma}$$ **(6)**

299

300   where ε is the dielectric constant of the passive film (a value of 60 has been assumed for

301   the passive film formed on Ti [15]), ε_0 is the vacuum permittivity ($8.85 \cdot 10^{-14}$ F/cm), *e* is

12

302 the electron charge ($1.60 \cdot 10^{-19}$ C) and σ is the positive slope of each straight line in the

303 M-S plots.

304

305 The values of N_D are presented in **Figure 7** for different LiBr solutions (0.1M, 0.5M,

306 3M and 11.42M) at 0.4 V. The results show that N_D values are of the order of 10^{19}-10^{20}

307 cm^{-3}, regardless the LiBr concentration, which is in agreement with those reported in the

308 literature for TiO$_2$ [10, 12].

309

310 An increase in LiBr concentration from 0.1M to 0.5M leads to a clear increase of N_D

311 (**Figure 7**). The PDM [38, 40, 55] assumes that the initial event that takes place at the

312 passive film/electrolyte interface in passivity breakdown is the occupation of surface

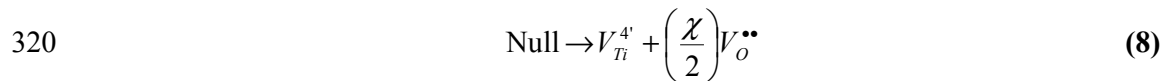313 oxygen vacancies by aggressive anions, such as bromides:

314

$$V_O^{\bullet\bullet} + Br^- \rightarrow Br_O^{\bullet} \tag{7}$$

315
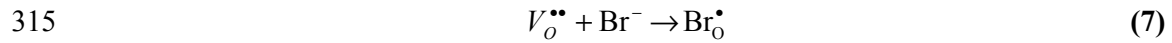
316

317 where $Br_O^{\bullet}$ represents a bromide anion adsorbed into an oxygen vacancy, $V_O^{\bullet\bullet}$, in the

318 film/electrolyte interface. This process is followed by a Schottky-pair type reaction:

319

$$Null \rightarrow V_{Ti}^{4'} + \left(\frac{\chi}{2}\right) V_O^{\bullet\bullet} \tag{8}$$

320

321

322 where V_{Ti}^{4} is a cation vacancy in the Ti passive film. Kroger-Vink notation is used for

323 the effective positive ($^{\bullet\bullet}$) and negative ($^{4'}$) charges in oxygen and cation vacancies,

324 respectively.

325

13

326 The adsorbed Br⁻ anions could desorb along with a surface cation to form a cation

327 vacancy/oxygen vacancy pair $(V_{Ti}^{4'} V_O^{\bullet\bullet})^{2'}$. This pair is subsequently annihilated, leading

328 to the formation of a subsurface cation vacancy and the regeneration of the surface $V_O^{\bullet\bullet}$:

329

$$\left(V_{Ti}^{4'} V_O^{\bullet\bullet}\right)'' \rightarrow \left(V_{Ti}^{4'}\right)_S + V_O^{\bullet\bullet} \qquad (9)$$
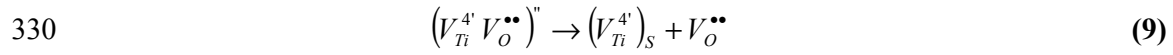
331

332 where the subscript S indicates a subsurface position in the passive film. The oxygen

333 vacancies continue reacting with additional Br^- at the film/electrolyte interface to

334 generate additional cation and oxygen vacancies. Hence, the generation of cation and

335 oxygen vacancies through eqs. (7)-(9) is autocatalytic.

336

337 Anion adsorption leads to the generation of cation vacancies at the film/solution

338 interface and hence to an enhancement in the flux of cation vacancies across the passive

339 film to the film/metal interface due to the outward movement (towards the passive

340 film/electrolyte interface) of cations in the film. If the flux of cation vacancies exceeds

341 the rate at which they are annihilated at the metal/film interface, the excess vacancies

342 will condense at the interface and the passive film will be locally detached from the

343 metal. As passive film dissolution continues, the film thins locally, eventually leading to

344 film breakdown [40].

345

346 According to the previous explanation, since oxygen vacancies are donor species, the

347 higher the donor density in the passive film, N_D, the lower the resistance to passivity

348 breakdown. This affirmation is in agreement with the values of the breakdown potential,

349 E_b, shown in **Table 2**, where $E_{b0.5M} < E_{b0.1M}$. However, when increasing the LiBr

350 concentration from 0.5M to 3M and 11.42M, N_D decreases, indicating that the higher

14

351 bromide concentration in the 3M and 11.42M LiBr solutions does not lead to a higher

352 degree of oxygen vacancies occupation by bromide ions. This result could explain the

353 lower susceptibility of Ti to undergo passivity breakdown in the 3M and 11.42M LiBr

354 solutions if compared with the 0.5M LiBr solution. Nevertheless, since the N_D values

355 obtained in concentrated LiBr solutions are still higher than that in the 0.1M LiBr

356 solution, this fact cannot satisfactorily explain the increase of E_b at high LiBr

357 concentrations or even the absence of passivity breakdown in the 11.42M LiBr solution.

358

359 The tendency of N_D with LiBr concentration also confirms that the differences

360 mentioned above in the steady-state current density (i_{SS}) with LiBr concentration are not

361 related to the density of donor species (oxygen vacancies and/or cation interstitials),

362 since $i_{SS0.1M} > i_{SS11.42M}$ but $N_{D0.1M} < N_{D11.42M}$.

363

364 **EIS measurements**

365

366 Mott-Schottky analysis has proved that the behavior of the passive film on Ti against

367 localized attacks in high LiBr concentrations is not directly related with its electronic

368 properties. **Figure 8** shows the experimental and simulated Nyquist diagrams for Ti in

369 0.1M, 0.5M, 3M and 11.42M LiBr solutions at 0.4 V. The experimental data have been

370 fitted to the electrical equivalent circuit shown in **Figure 9**, commonly used to account

371 for the bilayer structure of the passive film on Ti (porous outer layer and compact inner

372 layer) [4, 5, 56]

373

374 In all cases, Nyquist plots exhibit a typical passive state behavior characterized by

375 semicircular shape and high impedance values, suggesting that a highly stable film is

376 formed on all the electrodes [31-34].

377

378 An increase in LiBr concentration from 0.1M to 0.5M reduces the amplitude of the

379 semicircle in Nyquist plots, indicating a decrease of the total impedance of the system

380 and a loss in the protective properties of the passive film. This result is consistent with

381 the higher i_{SS} and N_D values obtained in the 0.5M LiBr solution. However, upon

382 increasing the bromide concentration to 3M and 11.42M, the total impedance increases

383 again, which agrees with the tendency of i_{SS} observed before (the lower the i_{SS}, the

384 higher the total impedance of the system), but differs in the case of N_D values (**Figure**

385 **7**), since the lowest N_D value (0.1M LiBr solution) does not imply the highest

386 impedance values.

387

388 The values of the equivalent circuit parameters are shown in **Table 3**. In this equivalent

389 circuit, R_S represents the solution resistance, the time constant at high frequencies

390 (R_1CPE_1) is related to the outer layer of the passive film (hydroxides), whereas the low-

391 frequency behavior (R_2CPE_2) is attributed to the inner layer (mainly TiO_2), more

392 compact than the outer one. Constant Phase Elements (CPEs) have been used instead of

393 pure capacitors, to describe the non-ideality of the system studied. CPEs have been

394 converted into pure capacitance, C, by using the following equation [57, 58]:

395

$$C = \frac{(Q \cdot R)^{1/\alpha}}{R} \qquad (10)$$

396

397

398   where Q is the impedance of the CPE and R corresponds to R_2 when determining

399   capacitance values of the second time constant in **Figure 9**. To determine C_1 from

400   CPE_1, R has been calculated as follows:

401

402 $$\frac{1}{R} = \frac{1}{R_S} + \frac{1}{R_1}$$ **(11)**

403

404   It can be observed from **Table 3** that the resistance values of the compact inner layer

405   (R_2) are significantly larger than the values associated with the outer porous layer (R_1),

406   which is consistent with the chosen physical model. These results indicate that the

407   protection provided by the passive film is predominantly due to the barrier layer. In

408   general, both the outer and inner layers exhibit similar capacitance values, of the order

409   of some $\mu F\ cm^{-2}$. Regarding the influence of LiBr concentration on the parameters, it

410   can be observed that R_1 decreases at high LiBr concentrations, while R_2 decreases from

411   0.1M to 0.5M but then it increases again, reaching the highest value in the 11.42M LiBr

412   solution. These results are in agreement with those obtained for i_{SS} (the lower the value

413   of i_{SS}, the higher the resistance of the barrier inner layer of the passive film, R_2).

414

415   According to the M-S results, the increase of R_2 in the 3M and 11.42M LiBr solutions

416   with respect to the value in the 0.1M LiBr solution cannot be related to the degree of

417   defectiveness of the passive film on Ti (**Figure 7 and Table 3**). This increase of R_2

418   could be explained in terms of the passive film dissolution and the influence of the

419   activity of water, a_W, on this process. Water is one of the reacting species in

420   electrochemical and corrosion mechanisms, but most corrosion works focus on the

421   properties of solutes whereas changes in the activity of water are rarely considered [33,

422   59]. Smart and Bockris [59] observed a decrease in the corrosion current density of iron

423   in concentrated chloride media with decreasing free water in the solution, that is, the

17

424   rate of iron dissolution (Fe/Fe^{2+}) was shown to strongly decrease with decreasing

425   activity of water. Hence, in the case of Ti in highly concentrated LiBr solution, the

426   decrease of a_W (**Table 1**) might lead to similar results. The reaction of dissolution of the

427   passive film formed on Ti by proton attack can be expressed as follows:

428

429    $$TiO_2 + 4H^+ \rightarrow Ti_{aq}^{4+} + 2H_2O \tag{12}$$
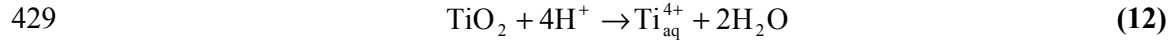
430

431   Although the activity of protons, a_{H+}, is constant, the concentration of H^+ will decrease

432   with decreasing free water (decreasing a_W). Therefore, the dissolution reaction given by

433   eq. (12) not only depends on pH (a_{H+}) but also on the number on H^+ at the passive

434   film/electrolyte interface, which in turn depends on a_W. Passive film dissolution is a

435   necessary step for passivity breakdown to occur, causing the thinning and subsequent

436   rupture of the passive film [40, 60]. Therefore, if passive film dissolution is somehow

437   hampered, for example by reducing the activity of water, passivity breakdown will

438   appear at higher potentials. This fact would explain the increase of E_b in highly

439   concentrated LiBr solutions (**Table 2**).

440

441   On the other hand, the formation of the precipitated outer layer ($TiO_2 \cdot nH_2O$) via the

442   hydrolysis of Ti^{4+} cations ejected from the inner layer (eq. (12)) also depends on a_W:

443

444 $$Ti_{aq}^{4+} + (n+2)H_2O \rightarrow TiO_2 \cdot nH_2O + 4H^+ \tag{13}$$
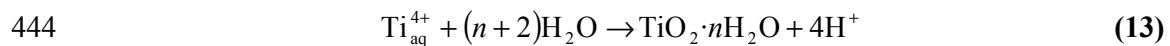
445

446   In fact, the values of the outer layer resistance, R_l, are higher in the 0.1M and 0.5M

447   LiBr solutions (**Figure 7**), indicating that the formation of precipitated hydroxides is

448   favored when a_W values are close to unity (**Table 1**).

18

449   However, the explanations given above concerning the dissolution of the passive film

450   do not completely explain why this behavior has not been observed, for example, in

451   stainless steels in highly concentrated LiBr solutions [35, 61, 62]. Apart from the

452   process of passive film dissolution (eq. (12)), there must be other Ti-specific surface

453   processes which are influenced by the decrease of a_W in highly concentrated LiBr

454   solutions. Davydov [37] suggested that the formation of an intermediate complex

455   between a valve metal (such as Ti) and the aggressive anions   (Br⁻) and its interaction

456   with the metal oxide could restrict the process of metal dissolution. Following the

457   descriptions of Davydov [37], this complex is formed when a bromide anion adsorbs on

458   a surface oxygen vacancy (eq. (7)) and then interacts with a Ti cation in the passive film

459   (Ti$_{Ti}$), according to the following reaction:

460

461
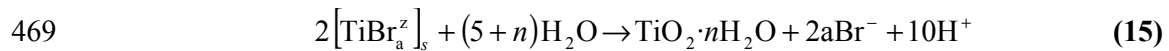$$\text{Ti}_{\text{Ti}} + a\text{Br}_{\text{O}}^{\bullet} \rightarrow \left[\text{TiBr}_{a}^{z}\right]_{s} + n\text{e}^{-} \tag{14}$$
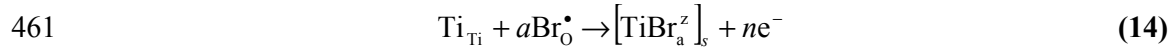
462

463   where $z = n + a$ and $\left[\text{TiBr}_{a}^{z}\right]_{s}$ is the surface complex. Along with the complex formation,

464   a cation vacancy/anion vacancy pair is also generated via a Schottky-pair type reaction,

465   eq. (8). The hydrolysis of the complex will break the bond with the passive film, thus

466   favoring the process of dissolution with the formation of the product of activated

467   dissolution, TiO$_2$·nH$_2$O:

468

469
$$2\left[\text{TiBr}_{a}^{z}\right]_{s} + (5+n)\text{H}_2\text{O} \rightarrow \text{TiO}_2 \cdot n\text{H}_2\text{O} + 2a\text{Br}^- + 10\text{H}^+ \tag{15}$$

470

471   As in the case of eq. (12), a decrease in the content of free water (i.e. decrease in a_W)

472   will slow down the process of hydrolysis and, as a consequence, the full process of

473   passivity breakdown.

474

**Influence of solvent and solute on the activity of water and passivity breakdown**

476

In order to verify that the decrease of the activity of water is responsible for the decrease

of the susceptibility of Ti to undergo passivity breakdown in highly concentrated LiBr

solutions, additional electrolytes have been used to study the electrochemical behavior

of Ti. In the first case, the activity of water has been reduced by adding different

amounts of methanol to a 0.5M LiBr aqueous solution. a_W values in these solutions have

been estimated from literature [63] taking the values of a_W shown in **Table 1** as starting

point: water-free methanol solution ($a_W \approx 0$), 50 mol% water – 50 mol% methanol ($a_W \approx$

0.60) and 70 mol% water – 30 mol% methanol ($a_W \approx 0.76$). In the second case, the

activity of water has been increased by changing the bromide salt (LiBr was replaced by

KBr), since Li is the smallest alkali cation and it is most strongly hydrated, thus

reducing the amount of free water in the solution. A 3M KBr solution has been used,

whose molality m_{KBr} = 3.40 (mol KBr) (kg H_2O)$^{-1}$ is similar to that of a 3M LiBr

solution (m_{LiBr} = 3.77 (mol LiBr) (kg H_2O)$^{-1}$). The comparison of mean ionic activity

coefficients ($\gamma_{\pm}$) and activities of water (a_W) between LiBr and KBr solutions is shown

in **Figures 10a** and **10b**, respectively. It can be observed that $\gamma_{\pm}$ values are higher in

LiBr solutions than in KBr solutions in almost the whole range of molalities, while a_W

values are visibly lower for LiBr solutions than for KBr solutions at molalities higher

than 2 mol kg^{-1} (for 3M KBr and LiBr solutions, a_{W_KBr} = 0.89 and a_{W_LiBr} = 0.81).

495

Figure 11 shows the potentiodynamic polarization curves of Ti in a 0.5M LiBr solution

with different water-methanol mol%. It can be observed that the four curves present a

clear passive range, regardless the water and methanol content. However, in the water-

20

free methanol solution, this passive range is significantly narrower than in the other solutions. Burstein and Whillock [64], <mark>as well as Banas et al [65], studied the passive behavior of Ti and other metals in methanolic solutions, and they concluded</mark> that methanol was responsible for the process of Ti dissolution, according to:
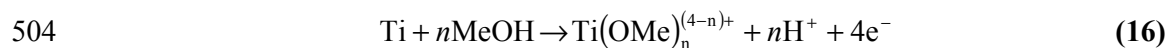
$$Ti + nMeOH \rightarrow Ti(OMe)_n^{(4-n)+} + nH^+ + 4e^- \tag{16}$$

In the presence of water, (50 mol% water, 70 mol% water and aqueous solution), Ti presents considerably wider passive regions than in the free-water methanol solution (**Figure 11**). Apart from the formation of TiO_2 due to direct reaction of Ti with water molecules, the dissolved complex of Ti(IV) formed according to eq. (16) could hydrolyze to form additional TiO_2 [64]:

$$Ti(OMe)_n^{(4-n)+} + 2H_2O \rightarrow TiO_2 + nMeOH + (4-n)H^+ \tag{17}$$
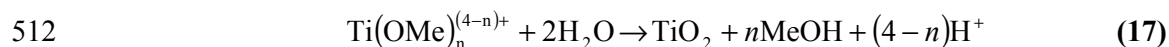
It is clearly observed in **Figure 11** that the breakdown potential in the water-methanol mixed solutions is significantly higher than in the aqueous solution (E_{b70_30} = 4.9±0.2 V; E_{b50_50} = 3.7±0.3 V; $E_{b\_aqueous}$ = 2.6±0.2 V). This increase in E_b can be explained taking into account the decrease of free water in the electrolyte (i.e. decrease in a_W), by partially replacing the aqueous solvent by the methanolic one. Thus, although methanol causes Ti dissolution (eq. (16)), the decrease of a_W slows down the dissolution of the electrode surface via eqs. (12) and/or (15), in a similar way as in highly concentrated LiBr solutions.

523   The potentiodynamic polarization curves of Ti in 3M KBr and 3M LiBr solutions are

524   presented in **Figure 12**. It can be observed that Ti is more susceptible to undergo

525   passivity breakdown in the 3M KBr solution ($E_{b\_KBr} = 2.6\pm0.2$ V) than in the 3M LiBr

526   solution ($E_{b\_KBr} = 3.3\pm0.3$ V). As it has been explained before, the mean ionic activity

527   coefficient reaches higher values in LiBr than in KBr solutions due to the high charge

528   density of the small lithium ion (**Figure 10a**). The higher activity coefficients in LiBr

529   solutions result in higher activity of bromide anions (a_{Br^-} in the 3M KBr solution is 2.0

530   and a_{Br^-} in the 3M LiBr solution is 6.6). As stated in eq. (4), the value of E_b should be

531   higher in the 3M KBr solution than in the 3M LiBr solution, since a_{Br^-} is significantly

532   lower in the former electrolyte. However, the higher values of $\gamma_\pm$ in the LiBr solutions

533   indicate a very strong interaction between water and ions, which lead to a decrease of

534   a_W (**Figure 10b**). Again, the reduction of a_W in the 3M LiBr solution restricts the

535   process of dissolution of the Ti surface (eqs. (12) and/or (15)), thus delaying the onset

536   of stable passivity breakdown.

537

538   **Relationship between E_b and a_W in concentrated LiBr solutions**

539

540   The linear relationship with positive slope found between E_b and log a_{Br^-} in highly

541   concentrated LiBr solutions (**Figure 3**) provides an empirical equation to evaluate E_b in

542   function of the activity of bromide anions. However, according to the previous results, it

543   is more coherent to relate E_b to the activity of water, a_W, since it is this parameter that

544   directly affects the value of E_b in these concentrated media. Starting from eqs. (1) and

545   (2), the activity of water can be expressed in terms of a_{Br^-}:

546

547
$$\log a_W = \frac{-\phi M_W \nu \dfrac{a_{Br^-}}{\gamma_{\pm}}}{2.303 \cdot 1000} = \frac{-\phi \cdot 18 \cdot 2 \dfrac{a_{Br^-}}{\gamma_{\pm}}}{2.303 \cdot 1000} = \frac{-A\phi a_{Br^-}}{\gamma_{\pm}} \qquad \textbf{(18)}$$

548

549   On the other hand, a_{Br^-} can be expressed in terms of E_b by using the linear relationship

550   E_b vs. $\log a_{Br^-}$ mentioned above (**Figure 3**):

551

552
$$a_{Br^-} = 10^{\frac{E_b - 2.50}{0.93}} \qquad \textbf{(19)}$$

553

554   Substituting eq. (19) into eq. (18):

555

556
$$-\log a_W = \frac{A\phi}{\gamma_{\pm}} 10^{\frac{E_b - 2.50}{0.93}} \rightarrow \log(-\log(a_W)) = \log\left(\frac{A\phi}{\gamma_{\pm}}\right) + \left(\frac{E_b - 2.50}{0.93}\right)$$

557

558   Finally, solving for E_b yields:

559

560
$$E_b = 0.93 \cdot \left[(\log(-\log(a_W))) - \log\left(\frac{A\phi}{\gamma_{\pm}}\right) \right] + 2.50 \qquad \textbf{(20)}$$

561

562   Eq. (20) relates the value of E_b to a logarithmic function of a_W. **Figure 13** shows the

563   experimental and calculated values of E_b as a function of a_W in concentrated LiBr

564   solutions. It can be observed that both experimental and calculated values of E_b are

565   similar, indicating that eq. (20) can be used to satisfactorily calculate the breakdown

566   potential of Ti in concentrated LiBr solutions ($m_{LiBr} > \sim 0.7$ mol kg^{-1}) as a function of

567   the activity of water.

568

569   Finally, it is necessary to explain why Ti did not undergo passivity breakdwon in the

570   11.42M LiBr solution. According to eq. (20), the breakdown potential of Ti in the

571   11.42M LiBr solution ($a_W = 0.12$) should be 5.6 V. However, passivity breakdown was

572   not observed even at potentials as high as 9 V. The absence of localized attacks in this

573   solution can be explained by changes in the TiO_2 surface. The irreversible formation of

574   titanium peroxo species at sufficiently high potentials (normally higher than $3V_{Ag/AgCl}$)

575   has been reported in the literature [7, 8, 15]. The formation of Ti peroxo species may

576   result in a very thin insulating or dielectric layer [8, 15] which would form in the

577   hydrated (outer) part of the passive film above 3V [8]:

578

579    $$TiO_2 + OH^- \rightleftharpoons TiO_3 + H^+ + 2e^- \qquad \textbf{(21)}$$
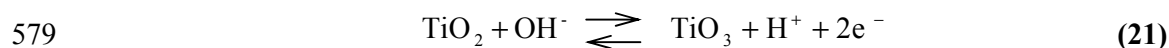
580

581   The presence of these species, such as TiO_3, can be noted by a yellowish color on the

582   electrode surface [8]. This yellow color was observed on the undamaged areas of all the

583   electrodes after the potentiodynamic polarization tests. However, the surface of the

584   electrode polarized in the 11.42M LiBr solution had a dark golden color. The color-

585   dependence of anodic Ti oxide layers on the polarization potential, and hence oxide

586   thickness, is a very well known phenomenon [66-73]. For example, it has been observed

587   [70, 71, 73] that at 5V the Ti surface has a light yellow color, while at 10-15V the

588   surface color changes to dark golden/brown. Hence, the absence of stable localized

589   attacks of Ti in the 11.42M LiBr solution can be attributed either to the formation of a

590   highly insulating or dielectric layer of Ti peroxo species at potentials higher than ~5V

591   (the value of E_p in the 8.06M LiBr solution is 4.7V) or/and to the increase of the Ti

592   oxide film thickness. Both phenomena could block the interaction between aggressive

593   anions and the surface of Ti, preventing passivity breakdown. This mechanism may be

594   similar to that reported by Sazou et al. [15] to explain passivity breakdown of Ti at high

595   potentials in the presence of high concentrations of chlorides. In any case, it is evident

596   that at sufficiently high potentials (higher than ~5V) the surface properties of the

597   titanium oxide change to such an extent that the risk of passivity breakdown is

598   completely eliminated, at least up to potentials as high as 9V.

599

600   **5. CONCLUSIONS**

601

602   A wide passive range where passive current density values (i_p) remained very low (of

603   the order of 1-3 $\mu A\ cm^{-2}$) was observed in all LiBr solutions, indicating the excellent

604   passive behavior of Ti. i_p values slightly increased with increasing LiBr concentrations

605   up to 0.7M LiBr, where i_p started to decrease until reaching its lowest value (1 $\mu A\ cm^{-2}$)

606   in the 11.42 LiBr solution.

607

608   In the low and moderately concentrated LiBr solutions, a decrease of E_b with increasing

609   bromide concentrations was observed, while in the more concentrated LiBr solutions, E_b

610   increased with increasing LiBr concentration. In the most concentrated LiBr solution

611   (11.42M) Ti did not undergo passivity breakdown under the experimental conditions

612   (up to 9 $V_{Ag/AgCl}$).

613

614   The steady-state passive current density, i_{SS}, was found to increase with Br^-

615   concentration at relatively low concentrations, but it decreased at high LiBr

616   concentrations, following the same tendency as i_p.

617

25

618   The passive film formed on Ti behaved as an *n*-type semiconductor, with the dominant

619   defects in the passive film being oxygen vacancies and/or Ti^{3+} interstitials. An increase

620   in LiBr concentration from 0.1M to 0.5M led to a clear increase of the donor density

621   (N_D), but when increasing the LiBr concentration from 0.5M to 3M and 11.42M, N_D

622   decreased. However, N_D values obtained in concentrated LiBr solutions were still higher

623   than in the 0.1M LiBr solution, so the electronic properties of TiO_2 passive film could

624   not be used to satisfactorily explain the increase of E_b at high LiBr concentrations or the

625   absence of localized attacks in the 11.42M LiBr solution.

626

627   The resistance of the hydroxide outer layer of the passive film on Ti was higher in low

628   concentrated LiBr solutions, whereas the resistance of the barrier layer of the film was

629   found to be higher in concentrated LiBr solutions. These results could not be related to

630   the degree of defectiveness of the passive film on Ti, but seemed to be associated with

631   the passive film dissolution and the influence of the activity of water, a_W, on this

632   process.

633

634   The activity of water, a_W, was found to have a strong influence on the susceptibility of

635   Ti to undergo passivity breakdown. In view of the results, it may be concluded that a

636   decrease in this parameter was responsible for the increase of the breakdown potential

637   in highly concentrated LiBr solutions and water-methanol-LiBr mixtures. An empirical

638   correlation between E_b and a_W was obtained for Ti in concentrated LiBr solutions.

639

640   **ACKNOWLEDGEMENTS**

641

26

644

645

REFERENCES

647

648   [1]   J. Been, J. S. Grauman, in: *Uhlig's Corrosion Handbook,* 2nd ed., R.Winston
649   Revie (ed.), 863-885, Wiley Interscience, New York (2000).

650   [2]   E. Blasco-Tamarit, A. Igual-Muñoz, J. García-Antón, D. García-García,
651   Corros. Sci. **49**, 1000 (2007)

652   [3]   Y. Z. Huang, D. J. Blackwood, Electrochim. Acta **51**, 1099 (2005)

653   [4]   J. Pan, D. Thierry, C. Leygraf, Electrochim. Acta **41**, 1143 (1996)

654   [5]   S. L. d. Assis, S. Wolynec, I. Costa, Electrochim. Acta **51**, 1815 (2006)

655   [6]   J. R. Birch, T. D. Burleigh, Corrosion **56**, 1233 (2000)

656   [7]   E. Peláez-Abellán, L. Rocha-Sousa, W. D. Müller, A. C. Guastaldi, Corros.
657   Sci. **49**, 1645 (2007)

658   [8]   K. Azumi, M. Seo, Corros. Sci. **43**, 533 (2001)

659   [9]   V. A. Alves, R. Q. Reis, I. C. B. Santos, D. G. Souza, T. d. F. Gonçalves, M.
660   A. Pereira-da-Silva, A. Rossi, L. A. da Silva, Corros. Sci. **51**, 2473 (2009)

661   [10] A. M. Schmidt, D. S. Azambuja, E. M. A. Martini, Corros. Sci. **48**, 2901
662   (2006)

663   [11] M. C. K. Sellers, E. G. Seebauer, Thin Solid Films **519**, 2103 (2011)

664   [12] Z. Jiang, X. Dai, H. Middleton, Mater. Chem. Phys. **126**, 859 (2011)

665   [13] D. S. Kong, W. H. Lu, Y. Y. Feng, Z. Y. Yu, J. X. Wu, W. J. Fan, H. Y. Liu, J.
666   Electrochem. Soc. **156**, C39 (2009)

667   [14] B. Roh, D. D. Macdonald, Russ. J. Electrochem. **43**, 125 (2007)

668   [15] D. Sazou, K. Saltidou, M. Pagitsas, Electrochim. Acta **76**, 48 (2012)

669   [16] P. R. Roberge, *Handbook of Corrosion Engineering*, p. 756, McGraw-Hill,
670   New York (2000).

671   [17] S. B. Basame, H. S. White, J. Phys . Chem. **99**, 16430 (1995)

672   [18]   S. B. Basame, H. S. White, J. Electrochem. Soc. **147**, 1376 (2000)

673   [19]   I. Dugdale, J. B. Cotton, Corros. Sci. **4**, 397 (1964)

674   [20]   S. Virtanen, C. Curty, Corrosion **60**, 643 (2004)

675   [21]   J. L. Trompette, L. Massot, L. Arurault, S. Fontorbes, Corros. Sci. **53**, 1262
676   (2011)

677   [22]   N. Casillas, S. Charlebois, W. H. Smyrl, J. Electrochem. Soc. **141**, **636** (1994)

678   [23]   T. R. Beck, J. Electrochem. Soc. **120**, 1310 (1973)

679   [24]   S. Huo, X. Meng, Corros. Sci. **31**, 281 (1990)

680   [25]   R. M. Fernández-Domene, E. Blasco-Tamarit, D. M. García-García, J. García-
681   Antón, Electrochim. Acta **58**, 264 (2011)

682   [26]   P. Srikhirin, S. Aphornratana, S. Chungpaibulpatana, Renew. Sust. Energ.
683   Rev. **5**, 343 (2001)

684   [27]   R. J. Lee, R. M. DiGuilio, S. M. Jeter, A. S. Teja, ASHRAE Tran. **96**, pt. 1
685   (1990)

686   [28]   J. L. Guiñón, J. García-Antón, V. Pérez-Herranz, G. Lacoste, Corrosion **50**,
687   240 (1994)

688   [29]   G. A. Florides, S. A. Kalogirou, S. A. Tassou, L. C. Wrobel, Energ. Convers.
689   Manage. **44**, 2483 (2003)

690   [30]   R. D. Misra, P. K. Sahoo, A. Gupta, Int. J. Refrig. **28**, 331 (2005)

691   [31]   W. J. Hamer, Y.-C. Wu, J. Phys. Chem. Ref. Data **1**, 1047 (1972)

692   [32]   J. M. Prausnitz, R. N. Lichtenthaler, and E. G. Azevedo, *Molecular*
693   *Thermodynamics of Fluid-Phase Equilibria*, p. 517, Prentice Hall, Upper
694   Saddle River, NJ (1999).

695   [33]   M. J. Blandamer, J. B. F. N. Engberts, P. T. Gleeson, J. C. R. Reis, Chem. Soc.
696   Rev. **34**, 440 (2005)

697   [34]   H. Selcuk, J. J. Sene, M. V. Zanoni, H. Z. Sarikaya, M. A. Anderson,
698   Chemosphere **54**, 969 (2004)

699   [35]   A. Igual-Muñoz, J. García-Antón, J. L. Guiñón, V. Pérez-Herranz,
700   CORROSION **59**, 606 (2003)

701   [36]   M. J. Muñoz-Portero, J. García-Antón, J. L. Guiñón, R. Leiva-García, Corros.
702   Sci. **53**, 1440 (2011)

703   [37]   A. D. Davydov, Electrochim. Acta **46**, 3777 (2001)

704 [38] L. F. Lin, C. Y. Chao, D. D. Macdonald, J. Electrochem. Soc. **128**, 1194
705 (1981)

706 [39] T. Haruna, D. D. Macdonald, J. Electrochem. Soc. **144**, 1574 (1997)

707 [40] D. D. Macdonald, J. Electrochem. Soc. **139**, 3434 (1992)

708 [41] D. D. Macdonald, Pure Appl. Chem. **71**, 951 (1999)

709 [42] D. D. Macdonald, Electrochim. Acta **56**, 1761 (2011)

710 [43] D. D. Macdonald, A. Sun, Electrochim. Acta **51**, 1767 (2006)

711 [44] K. Park, S. Ahn, H. Kwon, Electrochim. Acta **56**, 1662 (2011)

712 [45] D. D. Macdonald, J. Nucl. Mater. **379**, 24 (2008)

713 [46] A. D. Paola, Electrochim. Acta **34**, 203 (1989)

714 [47] W. P. Gomes, D. Vanmaekelbergh, Electrochim. Acta **41**, 967 (1996)

715 [48] M. Da Cunha Belo, N. E. Hakiki, M. G. S. Ferreira, Electrochim. Acta **44**,
716 2473 (1999)

717 [49] N. E. Hakiki, S. Boudin, B. Rondot, M. Da Cunha Belo, Corros. Sci. **37**, 1809
718 (1995)

719 [50] L. Hamadou, A. Kadri, N. Benbrahim, Appl. Surf. Sci. **252**, 1510 (2005)

720 [51] T. L. S. Wijesinghe, D. J. Blackwood, Corros. Sci. **50**, 23 (2008)

721 [52] J. Amri, T. Souier, B. Malki, B. Baroux, Corros. Sci. **50**, 431 (2008)

722 [53] D. G. Li, J. D. Wang, D. R. Chen, Electrochim. Acta **60**, 134 (2012)

723 [54] R. M. Fernández-Domene, E. Blasco-Tamarit, D. M. García-García, J. García-
724 Antón, Electrochim. Acta **95**, 1 (2013)

725 [55] M. Urquidi-Macdonald, D. D. Macdonald, J. Electrochem. Soc. **136**, 961
726 (1989)

727 [56] A. M. Schmidt, D. S. Azambuja, Mater. Res. **9**, 387 (2006)

728 [57] G. J. Brug, A. L. G. van den Eeden, M. Sluyters-Rehbach, J. H. Sluyters, J.
729 Electroanal. Chem. **176**, 275 (1984)

730 [58] C. Valero Vidal, A. Igual-Muñoz, Electrochim. Acta **55**, 8445 (2010)

731 [59] N. G. Smart, J. O. Bockris, Corrosion **48**, 277 (1992)

732 [60] G.S. Frankel, J. Electrochem. Soc. **145**, 2186 (1998)

733 [61] R. M. Fernández-Domene, E. Blasco-Tamarit, D. M. García-García, J. García-
734 Antón, Int. J. Electrochem. Sc. **6**, 3292 (2011)

735 [62] E. Blasco-Tamarit, A. Igual-Muñoz, J. García-Antón, Corros. Sci. **49**, 4452
736 (2007)

737 [63] P. S. Crozier, R. L. Rowley, Fluid Phase Equilibr. **193**, 53 (2002)

738 [64] G. T. Burstein, G. O. H. Whillock, J. Electrochem. Soc. **136**, 1313 (1989)

739 [65] J. Banaś, B. Stypuła, K. Banaś, J. Światowska-Mrowiecka, M. Starowicz, U.
740 Lelek-Borkowska, J. Solid State Electr. **13**, 1669 (2009).

741 [66] K.O. Beck, Titanium anodizing process, US Patent 2,949,411 (1960)

742 [67] J.L. Delplancke, M. Degrez, A. Fontana, R. Winand, Surf. Technol. **16**, 153
743 (1982)

744 [68] E. Gaul, J. Chem. Educ. **70**, 176 (1993)

745 [69] Y.T. Sul, C.B. Johansson, Y. Jeong, T. Albrektsson, Med. Eng. Phys. **23**, 329
746 (2001)

747 [70] Z. M. Yan, T. W. Guo, H. B. Pan, J. J. Yu, Mater. Trans. **43**, 3142 (2002)

748 [71] C. Chen, J. Chen, C. Chao, W.C. Say, J. Mater. Sci. **40**, 4053 (2005)

749 [72] M.V. Diamanti, B. Del Curto, M. Pedeferri, Color Res. Appl. **33**, 221 (2008)

750 [73] A. Karambakhsh, A. Afshar, S. Ghahramani, P. Malekinejad, J. Mater. Eng.
751 Perform. **20**, 1690 (2011)

752

753

754

755

756

757

758

759

760

761

762

763 **Tables**

764

765 **Table 1. Physical properties of the different LiBr solutions used in this work.**

C_{LiBr}/mol l^{-1}	C_{LiBr}/g l^{-1}	m_{LiBr}/(mol LiBr) (kg H$_2$O)$^{-1}$	$\gamma_\pm$	a_{LiBr}	ϕ	a_W
0.05	4.34	0.05	0.93	0.05	0.95	1.00
0.10	8.68	0.10	0.80	0.08	0.94	1.00
0.30	26.05	0.31	0.76	0.23	0.95	0.99
0.50	43.42	0.51	0.75	0.39	0.97	0.98
0.70	60.79	0.72	0.77	0.56	1.00	0.97
1.15	100	1.20	0.84	1.01	1.07	0.95
3.00	260.52	3.77	1.75	6.60	1.53	0.81
4.61	400	5.69	3.56	20.26	1.93	0.67
8.06	700	11.18	21.89	222.82	2.95	0.34
11.42	992	15.15	154.00	2333.67	3.93	0.12

766

767

768 **Table 2. Values of passive current density (i_p) <mark>at 0.4 V</mark> and breakdown potential**

769 **(E_b) of Ti in different LiBr solutions, obtained from potentiodynamic polarization**

770 **curves.**

771

C_{LiBr}/mol l^{-1}	i_p/μA cm^{-2}	E_b vs (Ag/AgCl)/V
0.05	1.4 ± 0.1	3.8 ± 0.2
0.10	2.0 ± 0.2	3.2 ± 0.3
0.30	2.3 ± 0.2	2.7 ± 0.2
0.50	2.5 ± 0.3	2.6 ± 0.3
0.70	2.6 ± 0.1	2.2 ± 0.2
1.15	1.7 ± 0.1	2.7 ± 0.1
3.00	1.4 ± 0.1	3.3 ± 0.3
4.61	1.4 ± 0.1	3.8 ± 0.2
8.06	1.2 ± 0.1	4.7 ± 0.3
11.42	1.0 ± 0.2	-----

772
773
774
775
776
777
778
779
780
781
782
783
784

785   **Table 3. Values of the equivalent circuit parameters for Ti in the 0.1M, 0.5M, 3M**

786   **and 11.42M LiBr solutions.**

787

C_{LiBr}/mol l^{-1}	R_S/Ω cm^2	R_1/kΩ cm^2	C_1/µF cm^{-2}	α_1	R_2/kΩ cm^2	C_2/µF cm^{-2}	α_2	χ^2 (x10^{-3})
0.1	7 ± 1	23 ± 3	3.8 ± 0.8	0.91 ± 0.01	2391 ± 157	4.6 ± 0.5	0.78 ± 0.24	0.9
0.5	4 ± 0	28 ± 2	4.4 ± 0.7	0.90 ± 0.01	1804 ± 116	10.5 ± 0.4	0.89 ± 0.14	1.8
3	1 ± 0	19 ± 2	3.4 ± 0.5	0.91 ± 0.01	3144 ± 108	1.3 ± 0.3	0.94 ± 0.09	3.5
11.42	2 ± 0	16 ± 2	3.2 ± 0.6	0.94 ± 0.01	3280 ± 101	3.9 ± 0.4	0.87 ± 0.07	4.1

788
789
790
791
792
793
794
795
796
797
798
799
800
801
802
803
804
805
806
807
808
809
810
811
812
813
814
815
816
817
818
819
820
821
822
823
824
825
826
827
828
829
830

831   Tables captions
832

833   Table 1. Physical properties of the different LiBr solutions used in this work.

834

835   Table 2. Values of passive current density (i_p) at 0.4 V and breakdown potential (E_b) of Ti in different

836   LiBr solutions, obtained from potentiodynamic polarization curves.

837

838   Table 3. Values of the equivalent circuit parameters for Ti in the 0.1M, 0.5M, 3M and 11.42M LiBr

839   solutions.

840

841   Figures captions

842

843   Fig. 1. Potentiodynamic polarization curves of Ti in different LiBr solutions at 25º C; (a) low and

844   moderately concentrated LiBr solutions; (b) concentrated LiBr solutions.

845

846   Fig. 2. Images of the Ti electrode surface before and after the polarization tests in (a) 0.5M and (b)

847   11.42M LiBr solutions.

848

849   Fig. 3. Plots of E_b vs. log a_{Br^-} for Ti in the different LiBr solutions.

850

851   Fig. 4. Current density transients obtained after applying a potential step from a cathode value of -0.9 V

852   to a passive value of 0.4 V for Ti in different LiBr solutions (0.1M, 0.5M, 3M and 11.42M).

853

854   Fig. 5. Capacitance-potential curves obtained for Ti in 0.5M LiBr solution at 0.4 V and at different

855   frequencies.

856

857   Fig. 6. Mott-Schottky plots of the passive film formed on Ti in 0.1M, 0.5M, 3M and 11.42M LiBr

858   solutions at 0.4 V, obtained at a frequency of 10 kHz.

859

860   Fig. 7. Values of donor density (N_D) of the passive film on Ti in different LiBr solutions (0.1M, 0.5M, 3M

861   and 11.42M).

862 <mark>Fig. 8. Experimental and simulated Nyquist diagrams for Ti in 0.1M, 0.5M, 3M and 11.42M LiBr</mark>

863 <mark>solutions at 0.4 V.</mark>

864

865 Fig. 9. Electrical equivalent circuit used to fit the experimental EIS data.

866

867 Fig. 10. Comparison of (a) mean ionic activity coefficients ($\gamma_\pm$) and (b) activities of water (a_W) between

868 LiBr and KBr solutions.

869

870 Fig. 11. Potentiodynamic polarization curves of Ti in a 0.5M LiBr solution with different water-methanol

871 mol%.

872

873 Fig. 12. Potentiodynamic polarization curves of Ti in 3M KBr and 3M LiBr solutions.

874

875 Fig. 13. Experimental and calculated (using eq. (20)) values of E_b as a function of a_W in the highly

876 concentrated LiBr solutions.

877
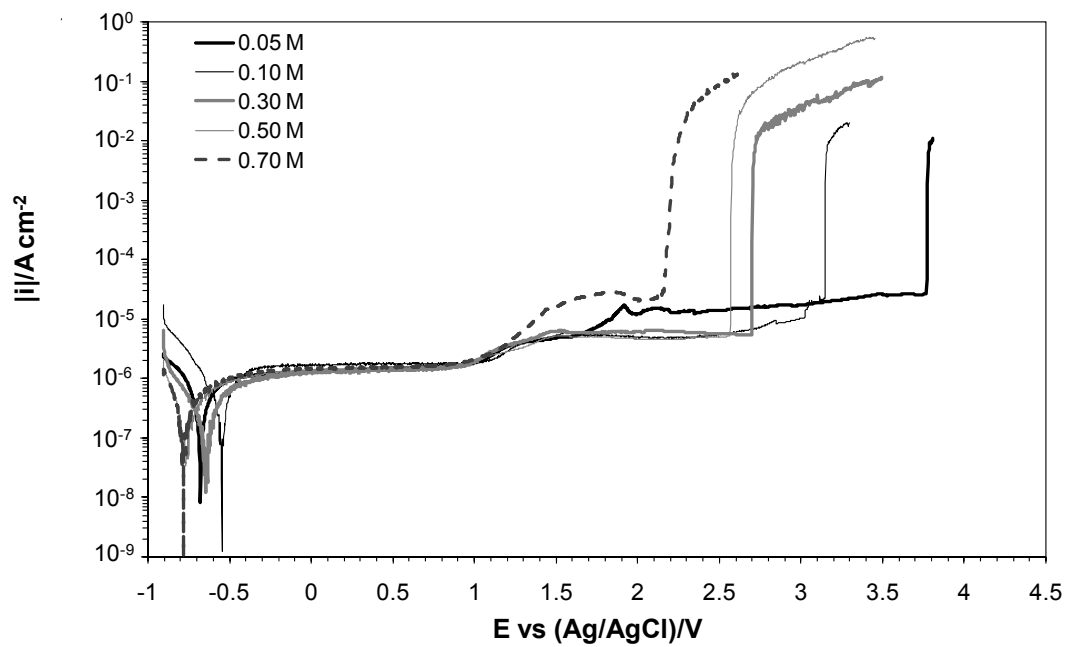
(a)
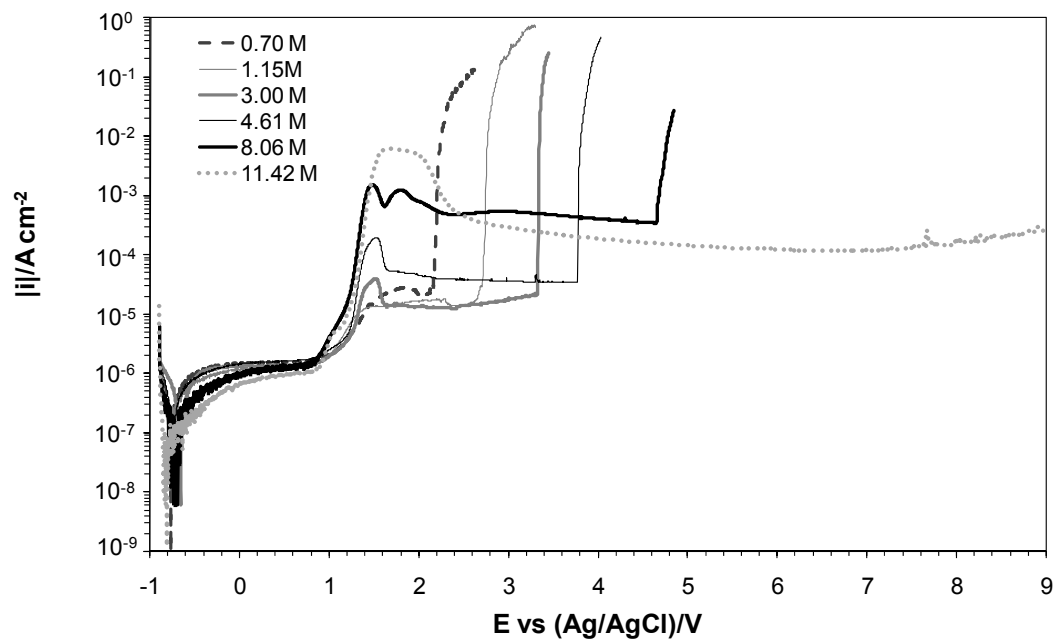
(b)
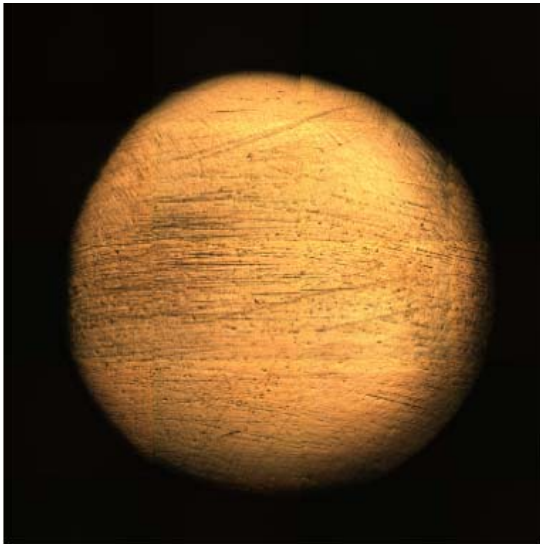
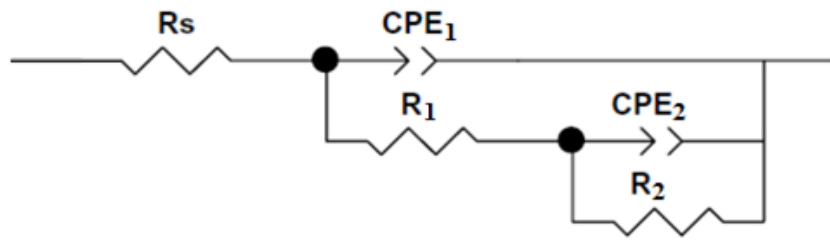**Initial mosaic (sample diameter = 8 mm)**   **Final mosaic (sample diameter = 8 mm)**

(a)

Initial mosaic (sample diameter = 8 mm)   **Final mosaic (sample diameter = 8 mm)**

(b)

(a)

(b)